

Ateneo de Manila University

Archium Ateneo

Physics Faculty Publications

Physics Department

10-30-2016

Cherenkov-Phase-Matched Nonlinear Optical Detection and Generation of Terahertz Radiation via GaAs With Metal-Coating

Ramon M. Delos Santos

Shinpei Ozawa


Valynn Magusara

Syougo Azuma

Anthony Tuico

See next page for additional authors

Follow this and additional works at: <https://archium.ateneo.edu/physics-faculty-pubs>

 Part of the [Optics Commons](#)

Authors

Ramon M. Delos Santos, Shinpei Ozawa, Valynn Magusara, Syougo Azuma, Anthony Tuico, Vernalyn Copa, Arnel Salvador, Kohji Yamamoto, Armando Somintac, Kazuyoshi Kurihara, Hideaki Kitahara, Masahiko Tani, and Elmer Estacio

Cherenkov-phase-matched nonlinear optical detection and generation of terahertz radiation via GaAs with metal-coating

RAMON DELOS SANTOS,^{1,2,*} SHINPEI OZAWA,³ VALYNN MAG-USARA,³ SYOUGO AZUMA,³ ANTHONY TUICO,¹ VERNALYN COPA,¹ ARNEL SALVADOR,¹ KOHJI YAMAMOTO,³ ARMANDO SOMINTAC,¹ KAZUYOSHI KURIHARA,⁴ HIDEAKI KITAHARA,³ MASAHIKO TANI,³ AND ELMER ESTACIO¹

¹National Institute of Physics, University of the Philippines, Diliman, Quezon City 1101, Philippines

²Department of Physics, Ateneo de Manila University, Loyola Heights, Quezon City 1108, Philippines

³Research Center for Development of Far-Infrared Region, University of Fukui, Fukui 910-8507, Japan

⁴Graduate School of Education, University of Fukui, Fukui 910-8507, Japan

*rdelossantos@nip.upd.edu.ph

Abstract: Terahertz (THz) wave detection and emission via Cherenkov-phase-matched nonlinear optical effects at 1.55- μm optical wavelength were demonstrated using a GaAs with metal-coating (M-G-M) and bare GaAs as a reference sample in conjunction with a metallic tapered parallel-plate waveguide (TPPWG). The metal-coated GaAs is superior to the bare wafer both as a THz electro-optic detector and as an emitter. Significant improvements in the detection and emission efficiency were obtained by utilizing a metal-coating due to better confinement and lower loss of the THz waves propagating in the M-G-M compared with bare GaAs.

© 2016 Optical Society of America

OCIS codes: (040.1880) Detection; (160.2100) Electro-optical materials; (040.2235) Far infrared or terahertz; (300.6495) Spectroscopy, terahertz; (190.7110) Ultrafast nonlinear optics; (230.7370) Waveguides.

References and links

1. Q. Wu and X. C. Zhang, "Ultrafast electro-optic field sensors," *Appl. Phys. Lett.* **68**(12), 1604–1606 (1996).
2. A. Leitenstorfer, S. Hunsche, J. Shah, M. C. Nuss, and W. H. Knox, "Detectors and sources for ultrabroadband electro-optic sampling: experiment and theory," *Appl. Phys. Lett.* **74**(11), 1516–1518 (1999).
3. Q. Chen, M. Tani, Z. Jiang, and X. C. Zhang, "Electro-optic transceivers for terahertz-wave applications," *J. Opt. Soc. Am. B* **18**(6), 823–831 (2001).
4. S. Ozawa, T. Nagase, S. Tsuzuki, D. Takeshima, T. Furuya, S. Nishizawa, K. Kurihara, F. Kuwashima, R. delos Santos, A. Somintac, E. Estacio, K. Yamamoto, M. Bakunov, and M. Tani, "Detection of THz radiation by using GaAs in Cherenkov-phase-matched electro-optic sampling," in *Proceedings of the 38th International Conference on Infrared, Millimeter and Terahertz Waves* (IEEE, 2013), pp. 1–2.
5. M. Tani, K. Horita, T. Kinoshita, C. T. Que, E. Estacio, K. Yamamoto, and M. I. Bakunov, "Efficient electro-optic sampling detection of terahertz radiation via Cherenkov phase matching," *Opt. Express* **19**(21), 19901–19906 (2011).
6. M. Tani, T. Kinoshita, T. Nagase, K. Horita, C. T. Que, E. Estacio, K. Yamamoto, and M. I. Bakunov, "Non-ellipsometric detection of terahertz radiation using heterodyne EO sampling in the Cherenkov velocity matching scheme," *Opt. Express* **21**(8), 9277–9288 (2013).
7. M. Nagai, K. Tanaka, H. Ohtake, T. Bessho, T. Sugiura, T. Hirosumi, and M. Yoshida, "Generation and detection of terahertz radiation by electro-optical process in GaAs using 1.56 μm fiber laser pulses," *Appl. Phys. Lett.* **85**(18), 3974–3976 (2004).
8. D. H. Auston, K. P. Cheung, J. A. Valdmanis, and D. A. Kleinman, "Cherenkov radiation from femtosecond optical pulses in electro-optic media," *Phys. Rev. Lett.* **53**(16), 1555–1558 (1984).
9. A. Rice, Y. Jin, X. F. Ma, X.-C. Zhang, D. Bliss, J. Larkin, and M. Alexander, "Terahertz optical rectification from $<110>$ zinc-blende crystals," *Appl. Phys. Lett.* **64**(11), 1324–1326 (1994).
10. K. Suizu, T. Shibuya, T. Akiba, T. Tutui, C. Otani, and K. Kawase, "Cherenkov phase-matched monochromatic THzwave generation using difference frequency generation with a lithium niobate crystal," *Opt. Express* **16**(10), 7493–7498 (2008).
11. M. Theuer, G. Torosyan, C. Rau, R. Beigang, K. Maki, C. Otani, and K. Kawase, "Efficient generation of Cherenkov-type terahertz radiation from a lithium niobate crystal with a silicon prism output coupler," *Appl. Phys. Lett.* **88**(7), 071122 (2006).

12. S. Ya. Tochitsky, J. E. Ralph, C. Sung, and C. Joshi, "Generation of megawatt-power terahertz pulses by noncollinear difference-frequency mixing in GaAs," *J. Appl. Phys.* **98**(2), 026101 (2005).
13. R. J. Dietz, B. Globisch, H. Roehle, D. Stanze, T. Göbel, and M. Schell, "Influence and adjustment of carrier lifetimes in InGaAs/InAlAs photoconductive pulsed terahertz detectors: 6 THz bandwidth and 90dB dynamic range," *Opt. Express* **22**(16), 19411–19422 (2014).
14. L. C. Chen and W. H. Fan, "Numerical simulation of terahertz generation and detection based on ultrafast photoconductive antennas," *Proc. SPIE* **8195**, 81950K (2011).
15. T. A. Liu, M. Tani, M. Nakajima, M. Hangyo, and C. L. Pan, "Ultrabroadband terahertz field detection by photoconductive antennas based on multi-energy arsenic-ion-implanted GaAs and semi-insulating GaAs," *Appl. Phys. Lett.* **83**(7), 1322–1324 (2003).
16. Y. S. Lee, *Principles of Terahertz Science and Technology* (Springer Science and Business Media, 2009), Chap. 3.
17. I. Wilke and S. Sengupta, "Nonlinear optical techniques for terahertz pulse generation and detection - optical rectification and electrooptic sampling," in *Terahertz Spectroscopy: Principles and Applications*, S. L. Dexheimer, ed. (Chemical Rubber Company, 2007), pp. 41–72.
18. A. Schneider, M. Stillhart, Z. Yang, F. Brunner, and P. Günter, "Improved emission and coherent detection of few-cycle terahertz transients using laser pulses at 1.5 μm ," *Proc. SPIE* **6582**, 658211 (2007).
19. S. P. Mickan and X. C. Zhang, "T-ray sensing and imaging," *Int. J. High Speed Electron. Syst.* **13**(2), 601–676 (2003).
20. M. Levinstein, S. Rumyantsev, and M. Shur, eds., "Handbook series on semiconductor parameters," <http://www.ioffe.rssi.ru/SVA/NSM/Semicond/GaAs/mechanic.html#Phonon>, accessed last January 21, 2016.
21. R. W. Boyd, *Nonlinear Optics* (Academic, 2003), Chap. 1.
22. B. E. A. Saleh and M. C. Teich, *Fundamentals of Photonics* (John Wiley and Sons, Inc., 1991), Chap. 18.
23. S. Tsuzuki, D. Takeshima, T. Sakon, T. Kinoshita, T. Nagase, K. Kurihara, K. Yamamoto, F. Kuwashima, T. Furuya, E. Estacio, K. Kawase, M. I. Bakunov, and M. Tani, "Highly sensitive electro-optic sampling of terahertz waves using field enhancement in a tapered waveguide structure," *Appl. Phys. Express* **7**(11), 112401 (2014).
24. S. Namba, "Electro-optical effect of zincblende," *J. Opt. Soc. Am.* **51**(1), 76–79 (1961).
25. R. Mendis and D. M. Mittleman, "Comparison of the lowest-order transverse-electric (TE_i) and transverse-magnetic (TEM) modes of the parallel-plate waveguide for terahertz pulse applications," *Opt. Express* **17**(17), 14839–14850 (2009).
26. E. S. Estacio, M. Hibi, K. Saito, C. T. Que, T. Furuya, F. Miyamaru, S. Nishizawa, K. Yamamoto, and M. Tani, "Saturation and polarization characteristics of 1.56 μm optical probe pulses in a LTG-GaAs photoconductive antenna terahertz detector," *J. Infrared Millim. Terahertz Waves* **34**(7–8), 423–430 (2013).

1. Introduction

The possibility of novel terahertz (THz) wave-based technology employing THz-time domain spectroscopy (THz-TDS) impels the development of efficient detectors and emitters that do not involve tedious preparation procedures. Terahertz detection via Pockels effect (electro-optic or EO sampling) [1–7] and emission via optical rectification (OR) [3, 7–12] have become popular in the field of THz photonics research as they do not require micro-fabrication and operate simply by exploiting the second-order nonlinear optical effects in a bulk nonlinear optical crystal. The EO detection scheme is a better alternative to the photoconductive detection since it does not suffer from carrier lifetime bottleneck that limits THz detection bandwidth in photoconductive antennas (PCAs) [13–15]. In THz-EO detection method, the THz electric field-induced birefringence in an EO crystal elliptically polarizes the probe pulse when they co-propagate inside the crystal [3,16]. The measured amount of change in ellipticity in terms of intensities of the two orthogonal polarization components of the probe beam determines the incident THz field strength [16]. Moreover, THz emission via OR is a nonlinear optical process that is based on difference frequency generation (DFG) of the various frequency components within the bandwidth of ultrashort laser pulses that are incident on a nonlinear optical crystal [9, 10, 16, 17]. The values of the interacting frequency components should be close to each other to produce an output wave at the difference frequency in the THz range.

For on-site commercial applications of THz-TDS, a femtosecond (fs) fiber laser of 1.55 μm wavelength is the most viable choice because it is cost-effective, portable and has stable oscillations compared to a conventional mode-locked Ti:Sapphire laser. In conjunction with the 1.55- μm fs fiber laser, the utilization of GaAs as a THz EO detector and as an emitter has several advantages including: 1) low THz absorption; 2) small mismatch between the optical

group and THz refractive indices; 3) relatively large second-order nonlinear optical susceptibility, and 4) well-established fabrication techniques due to the already existing technological platform for GaAs. It is expected that non-collinear Cherenkov-phase-matched detection and generation of THz waves in GaAs are feasible using a 1.55- μm fs fiber laser because it is transparent at this wavelength, and the crystal's optical group refractive index n_g (≈ 3.54 at 1.55 μm) and THz refractive index n_{THz} (≈ 3.595 at 1 THz) are close to each other [4, 7, 18, 19], making it possible to utilize GaAs without coupling optics in Cherenkov-phase matching scheme; unlike in crystals having large index mismatch in the optical and THz regions, such as LiNbO₃. GaAs is not strongly absorptive at the THz frequencies below the transverse optical (TO) phonon resonance (< 8 THz) [7,20] and it does not have an intrinsic birefringence [21,22]. Moreover since GaAs can be polished easily, it can be inserted directly into a metallic parallel plate waveguide (PPWG) coupled to a metallic, tapered waveguide that enhances Cherenkov-phase-matched EO sampling sensitivity [23]. These properties make GaAs an attractive nonlinear optical material for THz detection and generation. Table 1 summarizes the optical properties of GaAs in comparison with ZnTe and LiNbO₃, which are commonly used nonlinear optical crystals for detection and generation of THz radiation.

Table 1. Optical properties of LiNbO₃, ZnTe, and GaAs.

Crystal	r_{ij} (pm/V)	$n^3 r_{ij}$ (pm/V)	d_{ij} (pm/V)	Optical index n @ 1.55 μm	Group index n_g @ 1.55 μm	THz index n_{THz} @1THz	Cherenkov angle (deg.)
LiNbO ₃	$r_{33} = 30.9$	302	$d_{33} = 40$	$n_e = 2.138$	2.18	4.76	63.3
ZnTe	$r_{41} = 4.3$	88	$d_{14} = 94$	2.733	2.8	3.17	30.4
GaAs	$r_{41} = 1.8$	69	$d_{36} = 780$	3.374	3.54	3.595	10.0

In this study, THz wave detection and emission measurements were performed in the Cherenkov-phase-matched EO sampling [4–6] and OR, respectively, at 1.55 μm using metal-coated GaAs (M-G-M) and bare GaAs (BG) as reference sample. The samples were inserted into a metallic tapered PPWG (TPPWG). The comparison between the enhancement characteristics, both in THz detection and emission, of the M-G-M and the BG sandwiched in the TPPWG were investigated. Furthermore, polarization-dependent time domain measurements were carried out to study the efficiency in detecting and generating TM- and TE-polarized THz waves.

2. Experiment

The THz-TDS system that was used in Cherenkov-phase-matched EO sampling, as shown in Fig. 1, consists of a mode-locked fs fiber laser (Menlo Systems Inc. C-FIBER-780-SP-3) as the optical source, spiral PCA THz emitter and GaAs-EO crystal THz detector. The repetition rate of the laser is 100 MHz and the pulse width of the fundamental oscillations at 1.55 μm is about ~ 90 fs and that of the second harmonic generation (SHG) at 780 nm is about ~ 120 fs. The PCA was AC-biased ($20V_{\text{pp}}$ at 20 kHz) and pumped with a power of 18 mW by the SHG output (780 nm) of the 1.55- μm laser. The THz waves emitted by the PCA were elliptically polarized. The polarization direction of the 1.55 μm fundamental laser beam for the probe was controlled to optimize the EO sampling signal in terms of the modulation of probe beam due to different refractive indices for perpendicular and parallel polarizations induced by the THz electric field. The half-wave plate, placed before the GaAs-EO crystal, was used to prepare the 1.55- μm probe beam polarization direction. In particular, the polarization was tilted by 45° with respect to the z -axis ($<001>$ direction, which is vertical in the experimental setup shown in Fig. 1) of the GaAs crystal to measure TM-polarized THz waves. On the other hand, the probe beam polarization was at 0° or 90° with respect to the z -axis of the GaAs in order to detect TE-polarized THz radiation. The transmitted THz wave was detected by balanced detection scheme consisting of a half-wave plate, quarter-wave plate, polarizing

beam splitter (PBS) and a pair of Thorlabs DET10C InGaAs photo-diode detectors. It is noteworthy that when the incident power on a photodiode exceeds 1 mW, its output strongly saturates. Hence, the transmitted probe beam was attenuated to operate the balanced photodetectors well below the saturation level.

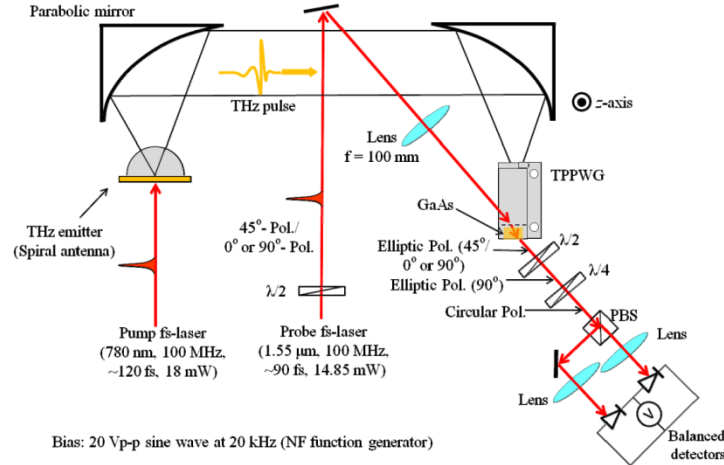


Fig. 1. Schematic of the experimental setup for detection of THz waves using GaAs-EO crystal with Cherenkov-phase-matched EO sampling in the balanced detection scheme. The probe beam polarization was at 45° and $0^\circ/90^\circ$ with respect to the z -axis of GaAs in order to detect TM- and TE-polarized THz waves, respectively.

In the optical probe configuration with the polarization at 45° with respect to the z -axis ($\langle 001 \rangle$ direction of GaAs), the GaAs EO sampling detector is only sensitive to the THz electric field parallel to the z -axis and the EO sampling signal $\Delta I/I$, which is the probe intensity modulation normalized by the incident probe intensity, is given by the following equation [24],

$$\frac{\Delta I}{I} = \Delta\Gamma = \frac{1}{2} \frac{\omega_{opt}}{c} r_{41} E_{THz}^{\parallel} d n_{opt}^3 = \frac{\Delta V}{\bar{V}} = \frac{V_A - V_B}{(V_A + V_B)/2} \quad (1)$$

where $\Delta\Gamma$ in Eq. (1) is the phase retardation induced by the EO effect, ω_{opt} is the angular frequency of the probe optical wave, c is the speed of light in vacuum, r_{41} is the EO coefficient, d is the EO crystal thickness, and n_{opt} is the optical refractive index of the GaAs crystal, and E_{THz}^{\parallel} is the THz electric field parallel to the z -axis, respectively. $\Delta V = V_A - V_B$ is the differential output voltage in the balanced detector detected with the lockin amplifier, which is synchronized with the emitter AC bias. $\bar{V} = (V_A + V_B)/2$ is the average DC output of the two balanced photodiodes, V_A and V_B . On the other hand, when the probe beam polarization was at 0° or 90° with respect to the z -axis, the GaAs EO sampling detector is only sensitive to the THz electric field perpendicular to the z -axis and the EO sampling signal, $\Delta I/I$, is expressed as [24]

$$\frac{\Delta I}{I} = \Delta\Gamma = \frac{\omega_{opt}}{c} r_{41} E_{THz}^{\perp} d n_{opt}^3 = \frac{\Delta V}{\bar{V}} = \frac{V_A - V_B}{(V_A + V_B)/2} \quad (2)$$

where E_{THz}^{\perp} in Eq. (2) is the THz electric field perpendicular to the z -axis. The difference between Eq. (1) and Eq. (2), which is a factor of $1/2$, is brought about by the difference in the orientation of the index ellipsoid and the associated change of the refractive index in the axes of ellipsoid when TM- or TE-polarized THz radiation is incident on the GaAs crystal.

Two (100) GaAs-EO crystal samples were used as THz detectors: 600 μm -thick bare GaAs (600 μm BG) and 600 μm -thick GaAs with metal-coat (600 μm M-G-M). Both samples are 6.5 mm x 3.5 mm in size [Fig. 2(a)]. The M-G-M sample is covered with aluminum film on all its facets, except on the (0 -1 -1) and (0 1 1) planes as shown in Fig. 2(a). Each sample was inserted into a TPPWG consisting of a tapered aluminum waveguide, which is connected to an aluminum PPWG as depicted in Fig. 2(b). Oil was used to fill the airgap between the surfaces of the sample and that of the PPWG. The THz beam was collimated and focused to the tapered waveguide by a pair of parabolic mirrors with off-axis focal length of 150 mm and normally incident to the (0, -1, -1) facet of the GaAs crystal (the 6.5 mm side is along the direction of the THz beam propagation). The 1.55- μm optical sampling beam was incident to the (0, -1, -1) facet of the crystal at the angle of 37°, to be transmitted inside the crystal at the Cherenkov phase-matching angle of 10° with respect to the THz wave as shown in Fig. 2(c).

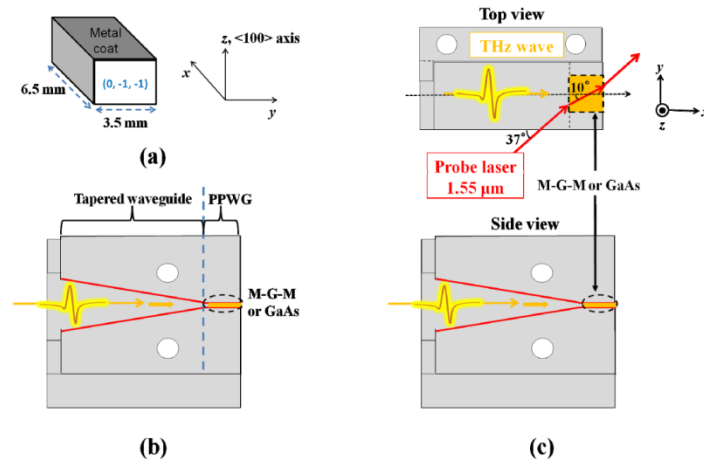


Fig. 2. (a) Size (not drawn into scale) and crystal orientation of the M-G-M sample, (b) structure of the TPPWG and (c) top view and side view of the TPPWG showing M-G-M or GaAs sample sandwiched between the walls of the PPWG section. The incident and refracted angles of THz and optical beams are also shown.

The polarization dependence of the THz-EO sampling scheme for the two samples was also investigated. The elliptically polarized THz waves from the spiral PCA was made to pass through a wire grid polarizer, inserted into the THz beam path between the parabolic mirrors, to exclusively select either the maximum TE- or the maximum TM-polarized components of the emitted THz radiation.

Figure 3 shows the schematic diagram of the experimental setup for THz emission via Cherenkov-phase-matching. In the experiment, the BG and M-G-M were photoexcited by the 1.55- μm fs fiber laser wherein the emitted THz waves were detected by the same spiral PCA that is optically switched by the SHG output (780 nm) of the laser. The polarization direction of the 1.55 μm laser beam was adjusted to optimize the Cherenkov THz radiation emitted by the samples. The THz radiation was collected by parabolic mirrors and fed to the PCA for time domain measurements. For the polarization-dependent measurements, a wire grid polarizer was inserted into the THz beam path between the parabolic mirrors.

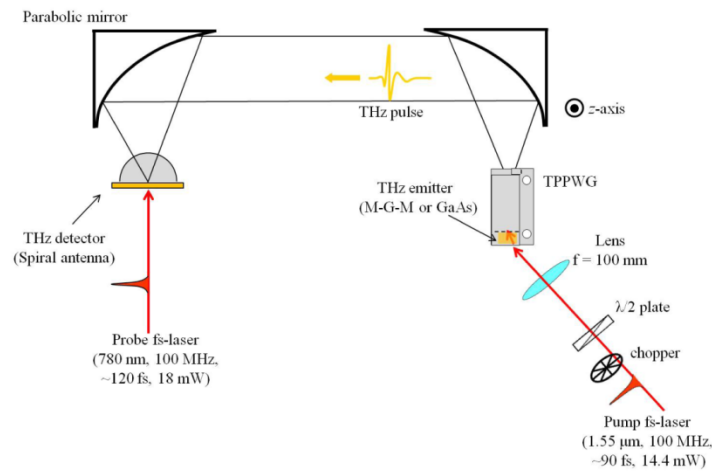


Fig. 3. Schematic of the experimental setup for Cherenkov-type generation of THz waves using GaAs crystal.

3. Results and discussion

The THz waveforms detected by Cherenkov-phase-matched EO sampling in the balanced detection scheme using the two GaAs-EO crystals inserted into the TPPWG are shown in Fig. 4. It has been reported that tapered waveguide coupled to a PPWG (collectively referred to as TPPWG) improves Cherenkov-phase-matched EO sampling sensitivity via THz electric field enhancement effect due to waveguiding on a subwavelength scale in the TPPWG [23]. Because of this subwavelength super-focusing effect, the THz electric field is concentrated in the narrow gap of metallic TPPWG compared to the diffraction-limited focusing. As long as the THz beam diameter focused by the parabolic mirror in the GaAs crystal is larger than the TPPWG exit gap, there is an enhancement of the THz electric field due to wave-guiding. The diameter of the THz beam spot focused by the parabolic mirror is 3 mm from the performed knife-edge measurement. Using Eq. (1) from Ref. 23, the calculated enhancement factor is approximately equal to 1.8 assuming a power transmission coefficient $T \approx 1$. On the other hand, the measured enhancement factor is 2.2 as shown in Fig. 4(a). Since this recent work compares metal-coated and bare GaAs, the measured and calculated field enhancement factors are not expected to be the same. The results in Fig. 4 simply illustrates that M-G-M coupled to a TPPWG (M-G-M/TPPWG) has better detection performance than BG/TPPWG. When the two samples were sandwiched between the walls of PPWG section of the TPPWG, the peak-to-peak EO signal from the sample with deposited metal increased to more than twice (~2.2 times) that of bare GaAs as shown in Fig. 4. Results strongly suggest that the more efficient detection is related to better THz wave-guiding in the PPWG with metal-coated GaAs. The metal coating in the M-G-M leads to enhanced THz wave-guiding characteristics compared with BG. When the BG is used in conjunction with the TPPWG, the gaps at the interfaces of GaAs and the metal waveguide act as wave trapping defects and deteriorate the propagation efficiency. Although oil is used to fill the gaps, crevices and voids between the GaAs and the metal walls of the PPWG section of TPPWG due to imperfections might have caused leakage of the THz waves significantly. In Fig. 4(b), the corresponding logarithmic THz amplitude spectra show that the detection efficiency is superior for M-G-M/TPPWG at all frequencies up to roughly 1.5 THz.

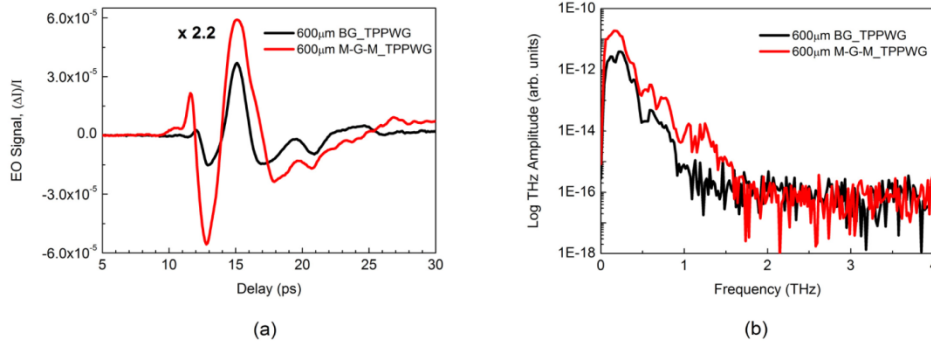


Fig. 4. (a) EO signals from 600 μm -thick bare GaAs and 600 μm -thick GaAs with metal-coat samples inserted into the TPPWG and (b) the corresponding logarithmic THz amplitude spectra. The peak frequency of the spectra is ~ 0.2 THz.

Polarization-sensitive detection measurements were performed to investigate exclusively the efficiency in detecting either TM- or TE-polarized THz waves. The polarization of the 1.55 μm fundamental laser beam for the probe was controlled to optimize the detection of TM- and TE-polarized THz radiation, independently. Since the relative amplitude of TE and TM components of the spiral PCA THz emission incident on the GaAs-EO detector is not known, the relative detection efficiencies for the TE- and TM-polarized THz waves cannot be compared. In general, the detection efficiency is better for the M-G-M sample compared to that of BG regardless of the THz wave polarization as shown in Figs. 5(a) and 5(b). This feature is again attributed to the better THz waveguiding in the TPPWG with the metal-coat of the M-G-M sample for both the TM- and TE-polarized THz radiation. For the TE-polarized THz waves, the detection sensitivity enhances with higher frequencies. This is ascribed to the decreasing attenuation coefficient with increasing frequency, which is a unique feature of this mode [25].

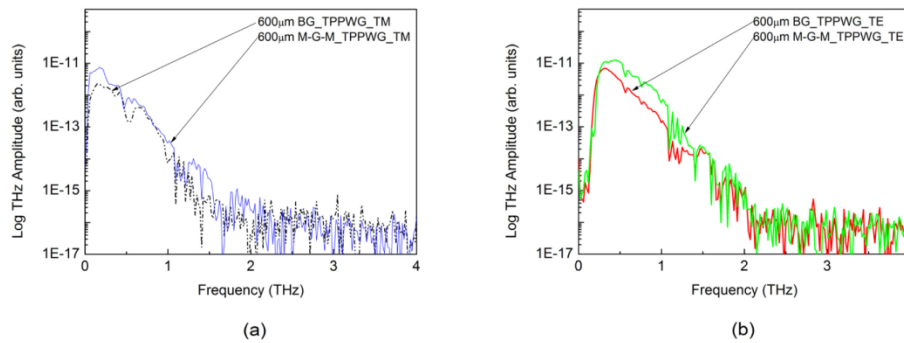


Fig. 5. Logarithmic THz amplitudes of (a) TM-polarized and (b) TE-polarized THz waves detected by 600 μm -thick bare GaAs and 600 μm -thick GaAs with metal-coat samples inserted into the TPPWG.

Based on Fig. 5(b), the 600 μm M-G-M and BG samples sandwiched between the walls of PPWG detected a cut-off frequency, f_c , of 0.195 THz for the TE-polarized THz waves. It is a well known fact that the TE modes in a PPWG have cut-off frequencies depending on the plate separation, while TM modes do not have a cut-off frequency. The theoretical value of f_c for the lowest-order transverse-electric (TE_1) mode of the PPWG is given by Eq. (3), where b is the plate separation and n is the refractive index of the medium between the plates [25].

$$f_c = \frac{c}{2nb} \quad (3)$$

When the THz beam is focused into the tapered section of the TPPWG, the aperture of the tapered waveguide connected to the PPWG causes the cut-off. Hence, it can be argued that $n = 1$ in Eq. (3) since the THz beam encounters this aperture in free-space. The calculated value of f_c is 0.250 THz. The exact origin of the discrepancy in the measured (~195 GHz) and theoretical (250 GHz) values of f_c is currently under investigation. But a plausible explanation may be due to the high refractive index of GaAs influencing the THz radiation incident on the facet of PPWG and lowering the actual cut-off frequency.

It is noteworthy that the finite diameter of the optical probe beam limits the potential THz bandwidth in noncollinear Cherenkov-phase-matched EO sampling since the phase of the THz wave is not constant over the entire optical beam diameter. When the optical probe beam crosses the THz beam at the Cherenkov angle 10° , different parts of the probe beam interact with the different phases of the THz wave. The diffraction-limited spot size diameter of the probe beam in the GaAs crystal is approximated by the equation given by [26]

$$W = \frac{4\lambda f M^2}{\pi D} \quad (4)$$

where, λ in Eq. (4) is the probe wavelength, f is the focal length of the lens (equal to 100 mm), M is the laser mode parameter and is taken to be 1 for Gaussian beams and D is the original diameter of the probe beam before focusing (equal to 4 mm). The calculated beam spot diameter of the probe beam is $49 \mu\text{m}$. This finite diameter value is the reason for the relatively low bandwidth of the detector since it prevents the detection of higher frequency components with half-wavelengths shorter than the probe beam diameter [5]. Furthermore, broadening (stretching) of the probe optical pulse possibly due to group velocity dispersion in GaAs can further restrict the detection bandwidth. This, however, is deemed to be negligible since the ~90 fs probe pulse is at least an order of magnitude narrower than the ps-wide THz pulse.

To further exemplify the efficacy of GaAs as a nonlinear crystal, Cherenkov-phase-matched generation of THz waves at 1.55- μm excitation was also carried out using the same samples. Figure 6 shows the time domain waveforms of Cherenkov THz radiation generated from the samples by optical pumping with the 1.55- μm fs-laser in the Cherenkov-phase-matched scheme. When both samples are used as THz emitters in conjunction with the TPPWG, the peak-to-peak signal from M-G-M is enhanced by a factor of 3.5 compared to that of BG as depicted in Fig. 6. The better THz generation efficiency from the M-G-M compared to the BG is attributed again to lower propagation loss of THz waves in the M-G-M sample.

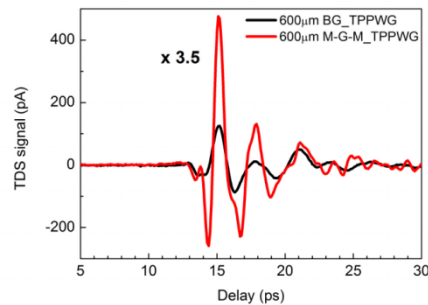


Fig. 6. Waveforms of Cherenkov THz radiation from 600 μm -thick bare GaAs and 600 μm -thick GaAs with metal-coat samples inserted into the TPPWG.

The spectra of the TM- and TE-polarized components of the emitted THz radiation from the samples are shown in Figs. 7(a) and 7(b), respectively. As in the EO detection experiment,

the polarization of the 1.55- μm laser beam was adjusted to optimize independently the TM- and TE-polarized THz generation. Regardless of the polarization, there is an enhanced efficiency in generating THz waves via the M-G-M sample as a result of better waveguiding of THz waves. It should be noted that the TE-polarized THz waves show a cut-off frequency at around 0.195 THz irrespective of the sample, which agrees with the experimentally observed cut-off frequency in the EO detection experiment.

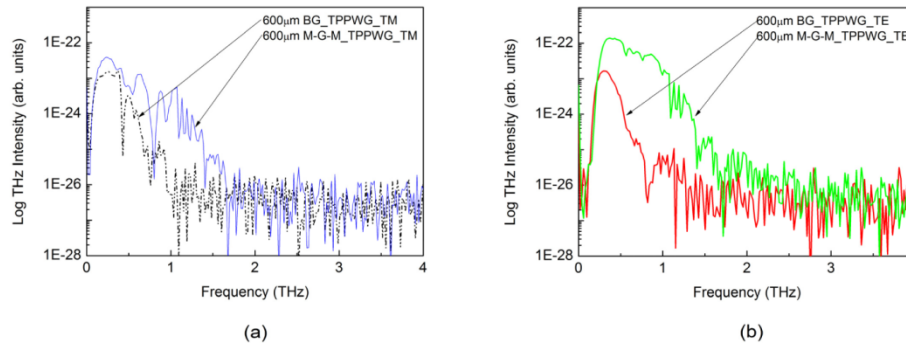


Fig. 7. Logarithmic THz intensities of (a) TM-polarized and (b) TE-polarized Cherenkov THz radiation from 600 μm -thick bare GaAs and 600 μm -thick GaAs with metal-coat samples inserted into the TPPWG.

A possible limitation of GaAs as a THz emitter via Cherenkov-phase-matching is the TO phonon bottleneck of the crystal at 8 THz. In THz emission via optical rectification process, the optical phonon resonances in an EO crystal are not available for THz generation due to strong absorption of THz radiation [17]. The reduction of the thickness of the GaAs crystal is expected to increase the emitted THz bandwidth [17]. For further optimization of the GaAs-EO crystal, it is important to find the optimal thickness of the crystal for practical implementation. One significant advantage of using metal-coated GaAs instead of MgO:LN in terms of THz emission performance is the significantly lower THz absorption for GaAs than in LN crystal.

4. Conclusion

We have demonstrated Cherenkov-phase-matched generation and detection of THz waves in GaAs at 1.55- μm excitation and optical sampling probe, respectively; in conjunction with a metallic TPPWG. When TPPWG was utilized, results show that M-G-M has much better performance than BG, both as an emitter and a detector. The improvement in the generation and detection efficiency of the M-G-M/TPPWG is attributed to better confinement and waveguiding of THz waves on M-G-M compared with BG. The result suggests the importance of the quality of the interfaces of a nonlinear crystal and the walls of metallic waveguide in generating and detecting THz waves when the crystal is used in conjunction with metallic waveguide structures.

Funding

Japan Science and Technology Agency (JST) Collaborative Research Based on Industrial Demand Program; Japan Society for the Promotion of Science (JSPS) Grant-in-Aid for Scientific Research (B)-Grant # 25286066; University of the Philippines (UP) System Emerging Interdisciplinary Research Program (OVPAE-EIDR-C06-04).